Article

On the Coupling of Electron Transfer to Proton Transfer at Electrified Interfaces

Aimin Ge,[⊥] Georg Kastlunger,[⊥] Jinhui Meng, Per Lindgren, Jia Song, Qiliang Liu, Alexander Zaslavsky, Tianquan Lian,* and Andrew A. Peterson*

Read Online

ACCESS | Metrics & More | Article Recommendations | Supporting Information

ABSTRACT: Many electrochemical processes are governed by the transfer of protons to the surface, which can be coupled with electron transfer; this electron transfer is in general non-integer and unknown *a priori*, but is required to hold the potential constant. In this study, we employ a combination of surface spectroscopic techniques and grand-canonical electronic-structure calculations in order to rigorously understand the thermodynamics of this process. Specifically, we explore the protonation/deprotonation of 4-mercaptobenzoic acid as a function of the applied potential. Using grand-canonical electronic-structure calculations, we directly infer the coupled electron transfer, which we find to be on the order of 0.1 electron per proton; experimentally, we also access this quantity via the potential-dependence of the pK_a. We show a striking agreement between the potential-dependence of the measured pK_a and that calculated with electronic-structure calculations.

We further employ a simple electrostatics-based model to show that this slope can equivalently be interpreted to provide information on the degree of coupled electron transfer or the potential change at the point of the charged species.
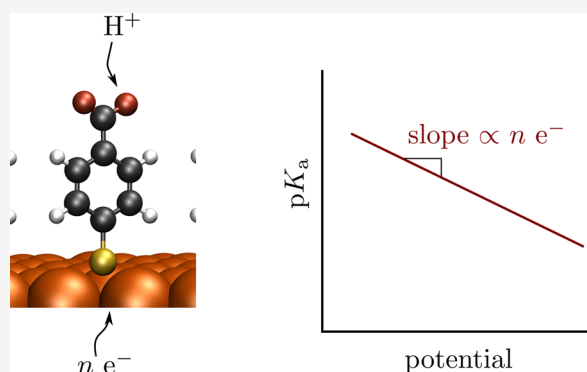
INTRODUCTION

The transfer of a proton to a surface or to a surface-adsorbed species is one of the most common reactions in electrochemistry. For example, many electrocatalytic or photoelectrocatalytic fuel formation reactions—such as H_2 evolution, CO_2 reduction, and water oxidation—involve proton-coupled electron-transfer reactions. When a species reacts at a surface held at a constant potential, an unknown and in general non-integer number of electrons must also be transferred; that is, a potentiostat keeps the potential constant by the flow of electrons.[1−3]

The pK_a of reacting species at the electrocatalyst surface is a key parameter that determines reaction mechanisms, and as we will show, the potential-dependence of the pK_a can provide direct information on the coupling of electron transfer to proton transfer. Interfacial acid−base equilibrium has attracted attention due to its importance in both fundamental research and practical applications.[4−10] Many intrinsic factors such as surface coverage,[11] substrate−molecule interaction,[12] and the curvature of the nanoparticles[13] are known to affect the acid dissociation at interfaces significantly. In an electrochemical reaction, however, the applied potential provides an externally controllable way to affect the acid dissociation.[6] Techniques such as voltammetry,[14−18] electrochemical impedance spectroscopy,[16] infrared spectroscopy,[19−21] and surface-enhanced Raman spectroscopy (SERS)[22,23] have been applied to

investigate the effects of applied potential on acid dissociation. Although it is now well established that the applied potential affects interfacial pK_a, the amplitude of this effect varies significantly among different reports and the underlying mechanism remains unclear.[19,20] Both electrical field-driven protonation/deprotonation[16,18] and potential-induced change of interfacial cation activity[19,20,22] have been proposed to explain the experimental observations.

While electronic-structure calculations have been used to study electrochemical interfaces for decades now, recently grand-canonical approaches have begun to gain popularity. In these approaches, the potential (manifested as the work function) is held constant by varying the number of electrons in the simulation. These calculations directly predict the (non-integer) number of electrons involved in elementary processes, and to our knowledge these predictions have not been validated against experiment. In this work, we attempt to unify the understanding of acid dissociation at the electrified interface, by combining experimental measurements using
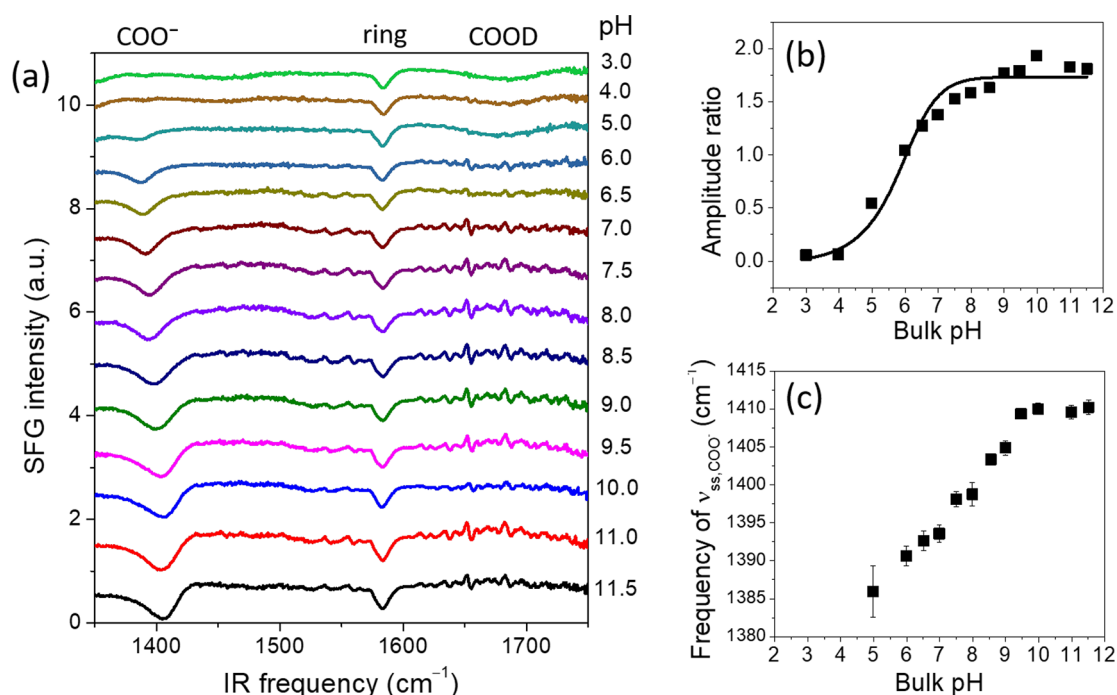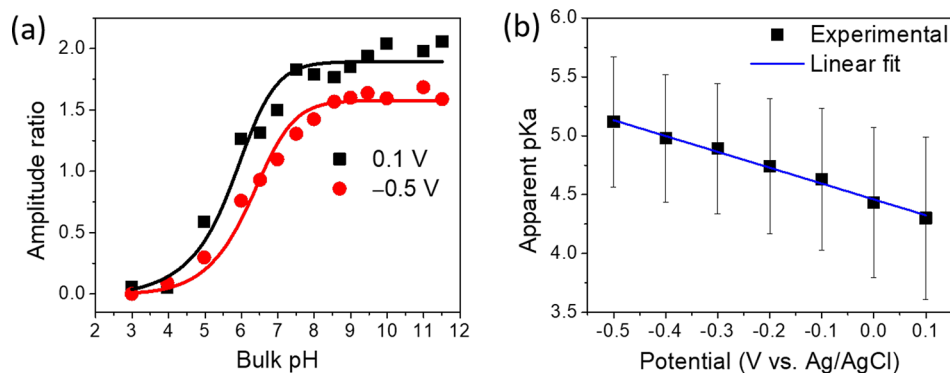
Figure 1. pH-dependent SFG spectra of 4-MBA SAM in D_2O buffer solutions without applying bias. (a) SFG spectra at indicated pH values. The spectra have been offset vertically for clarity. (b) SFG amplitude ratio between COO^- and ring modes and (c) frequency of COO^- as a function of bulk pH.

Figure 2. (a) Amplitude ratio (COO^-:ring) as a function of bulk pH at 0.1 V and −0.5 V vs Ag/AgCl. Symbols are experimental results; curves are fits according to eq 1. (b) pK_a^{ap} as a function of applied potential.

vibrational sum frequency generation (SFG) spectroscopy and electronic-structure calculations carried out in a constant-potential formulation. We will show how we can build on well-established models in electrochemical theory[1,24−32] with simple electrostatic models. As a model system we employ the potential-dependent acid−base equilibrium of 4-mercapto-benzoic acid (4-MBA) monolayers immobilized on a planar gold thin film, which experimentally allows us to use the vibrational mode of the molecule's ring as an internal reference of relative surface density.[8,33,34]

■ **RESULTS AND DISCUSSION**

We first describe how we used SFG to determine the apparent pK_a in the absence of applied external potential. Self-assembled monolayers (SAM) of 4-MBA were synthesized and measured with SFG in buffers at varied pH values; these SFG spectra and analyses are shown in Figure 1. Full methodological details are contained in Supporting Information sections S1.1−S1.3. The peaks around 1400, 1585, and 1670 cm^{-1} are assigned to the

symmetric stretch mode of COO^-, the phenyl ring mode, and the COOD mode, respectively.[35,36] It can be seen that with increasing buffer pH, the intensity of the COOD band decreases and the intensity of the COO^- band increases, while the intensity of the ring band shows much less pronounced changes. The amplitude ratio, f_{COO^-}, between the COO^- and ring bands is used to quantify the fraction of deprotonated carboxylate groups at different pH values, and thus find the apparent interfacial pK_a (pK_a^{ap}). Although the fraction of protonated/deprotonated species can also be obtained from the COOD band, there is a larger error in the determination of its amplitude because of its much broader width. A similar procedure has been used in previous studies.[8,22,33,34]

The data are fit to the following equation,[37−39]

$$pH - pK_a^{ap} = \log \frac{f_{COO^-}}{f_{COO^-}^{max} - f_{COO^-}} + \alpha \frac{f_{COO^-}}{f_{COO^-}^{max}} \qquad (1)$$

where α is a dimensionless number equivalent to $-\overline{E}/(\ln 10 \times RT)$, where $\overline{E}$ is the energy of interaction between charged molecules;[38] $f_{COO^-}^{max}$ is the maximal fraction of the deprotonated 4-MBA molecules. A best-fit procedure gives $pK_a^{ap} \approx 4.5$ and $\alpha \approx 0.9$, for these no-bias conditions. Deviations between the experimentally determined titration curves and the fit curves may in part be caused by the heterogeneity of the polycrystalline surfaces and the resulting SAM layers. The reported[12] pK_a of free 4-MBA is ~4.2; this shift is consistent with the reported shift of pK_a^{ap} between free and surface-immobilized carboxylic acids.[11−13,34]

To measure the effect of potential on the pK_a, we performed *in situ* SFG measurements as a function of applied potential at 14 pH values and repeated the above analysis. Figure 2a shows example data of the amplitude ratio as a function of pH at potentials of 0.1 and −0.5 V vs Ag/AgCl. The data were again fit to eq 1 and the fitted pK_a^{ap} values are shown in Figure 2b. We enforced that α take on a single value across all potentials rather than regressing this at each potential individually, since we physically expect this term to only be affected by the strength of the interaction between the charged groups. The pK_a^{ap} shifts from ~4.3 at 0.1 V to ~5.1 at −0.5 V; that is, the pK_a^{ap} of the 4-MBA immobilized on Au increases at more negative applied potentials.

What is the origin of this potential response? We will first note that a potentiostat keeps the potential at a fixed value ϕ by supplying or removing electrons, and the appropriate chemical reaction is written as

$$*AH + ne^- \xrightarrow{\phi} *A^{(1+n)-} + H^+ \tag{2}$$
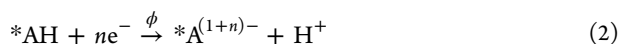
where n need not be an integer and can take on either a positive or negative sign. *A indicates the species bound to the surface. We note that the superscript "(1+n)−" refers to the net charge difference on the electrode−adsorbate system, and does not imply where the charge may localize. This electron transfer from the external circuit is sometimes referred to as the "electrosorption valency" or "formal partial charge transfer".[1,27−30,40]

As noted earlier, the value of n can readily be found by performing electronic-structure calculations in the (electronically) grand-canonical ensemble; that is, constant-potential calculations. We perform these calculations in the density functional theory formalism, using the solvated jellium (SJ) approach[41] to control the potential. Since the potential is kept constant in the calculations and number of electrons in the system is variable, n is inferred *a posteriori* simply by comparing the number of electrons in the acid and anion simulations at a given potential; that is, we neither assume n nor do we rely on arbitrary charge-partitioning methods.[42−44] When we perform such calculations, as described in more detail in Supporting Information section S1.4, we find n to be in the range of −0.05 to −0.3, depending upon the SAM density and tilt angle.

The SJ-DFT calculations also provide us with $\Delta G_{rxn}^\circ(\phi)$; that is, the potential-dependent free-energy change of reaction. With these values, we can calculate the apparent pK_a vs potential for differing surface packings and tilt angles, which is shown in Figure 3. Here, we see that the trends in the model systems nicely bracket those observed via SFG. The dominant potential-dependence of $\Delta G_{rxn}^\circ(\phi)$ comes from the term $-ne\phi$, as shown in Supporting Information section S3.1. We can therefore readily estimate the slope of pK_a vs applied potential; this slope is approximately
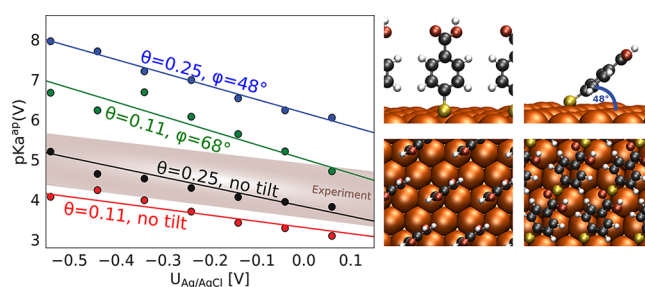
Figure 3. pK_a^{ap} versus the applied potential. θ indicates the surface coverage density, while φ indicates the tilt angle as shown.

$$\frac{dpK_a}{d\phi} \approx \frac{ne}{\ln 10 \times k_BT} \tag{3}$$

The slopes approximated with the above equation closely match those calculated from $\Delta G_{rxn}^\circ(\phi)$, indicating the potential-dependence can be attributed to the electron transfer n.

Previous literature has offered a different interpretation of the experimentally observed change in pK_a^{ap} with the applied potential.[14,15,22,45] In this interpretation, eq 4 represents the equilibrium between a neutral (*AH) and a charged (*A⁻) species at an interface, which may react differently in energy when the applied potential is changed.

$$*AH \rightarrow *A^- + H^+ \tag{4}$$

The third species, H⁺, is assumed to be in equilibrium with the bulk reservoir and is thermodynamically independent of the applied potential. However, the charge in *A⁻ sits some distance off of the electrode surface, where the local potential does not change with the full affect of the applied potential— that is, its energy will respond only to that portion of the applied potential felt at the point of the charge. From this viewpoint the response of pK_a to applied potential can be derived (Supporting Information section S3.2) to be

$$\frac{dpK_a}{d\phi} = \frac{-\delta e}{\ln 10 \times k_BT} \tag{5}$$

where δ is that fraction of the applied potential change manifested at the point charge. From the experimentally measured slope, we calculate $\delta \approx 0.1$, which we can interpret to mean that the point charge feels about 10% of changes to the surface potential; that is, the fraction of the potential drop across the dielectric 4-MBA monolayer is about 90%.

We can analyze this interpretation in the context of electronic-structure calculations. We compare *AH and *A⁻ at two different simulated applied potentials, as shown in Figure 4. The potential-drop profile is very similar for the protonated and deprotonated SAM. Three distinct regions can be identified in the potential profile. Starting from the electrode's surface to the right a high-field region appears which is a consequence of the less dense (nearly vacuum-like) layer of S-anchors. This region is followed by an intermediate field region, which can be envisioned as a dielectric arising from the backbone of the 4-MBA molecule. Finally, the double layer/diffuse layer region shows a comparatively low electric field as a consequence of the high screening due to the (implicit) solvent. It is at the interface between the intermediate- and low-field regions where the reaction center is located. If we take the reaction plane to be the center of the O−H bond (20.5 Å), we find a potential drop of 89%. These
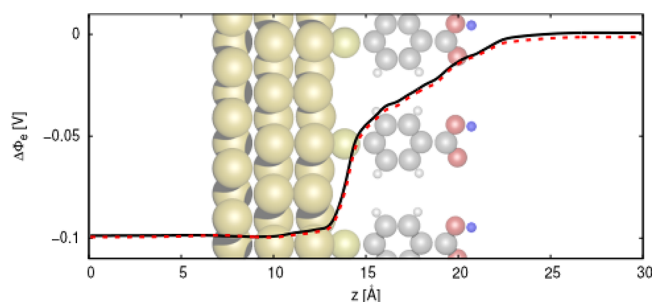
Figure 4. Electrostatic potential change at a potential difference of 0.1 V for both the protonated (black solid) and deprotonated (red dashed) SAMs at a coverage of $\theta = 0.25$. The proton absent in the anionic SAM structure is highlighted in blue.

results are also in close agreement with the experimental prediction.

Thus, two very different interpretations yield very similar expressions for the slope, and both can claim very strong agreement between experimental observations and differing aspects of the electronic-structure calculations. Can we unite the two interpretations, thus potentially giving broader insight into proton-transfer reaction thermodynamics at electrochemical interfaces?

In the remainder of this work, we develop a simplified purely electrostatic model to relate the approaches, following the precedent of many historical interpretations.[2,24,25,28,46,47]

A simple model of a charged interface is shown in Figure 5. In this one-dimensional model, the plane at $z = 0$ represents
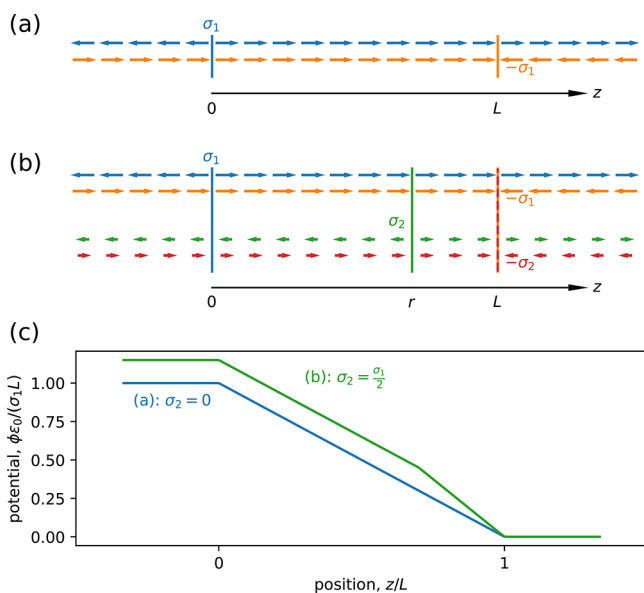
Figure 5. (a, b) Fields emanating from charged planes at 0, r, and L. (c) The potentials that result from integrating the net fields.

the electrode surface, which is physically where charge accumulates in a perfect conductor. A uniform charge density (that is, charge per area) of σ_1 is assigned to the $z = 0$ plane. This is balanced by a counter charge at $z = L$, which achieves charge neutrality. We will start by examining solely this system, shown in part (a) of the figure.

Gauss's law gives us the electric field emanating normal to any plane in our one-dimensional system as

$$E = \frac{\sigma}{2\varepsilon} \qquad (6)$$

where ε is the dielectric constant. This field emanates infinitely, in both directions from the plane. Fields from multiple charged planes are additive. Recall that the field is the (negative) gradient of the electric potential ϕ, so in the one-dimensional case (normal to the plane) $E = -\frac{d\phi}{dz}$, and we can find the potential change by integrating against the field. Thus, in this simple case a net field exists solely in $0 < z < L$, and we can readily obtain the potential at $z = 0$, as shown by the blue curve in Figure 5. This simple model—which is just a capacitor—allows us to readily see how the injection of a charge density σ_1 affects the potential at $z = 0$. (Capacitor models have been used elsewhere to understand electrochemical phenomena.[48−50])

Now consider the case where a charge σ_2 is added at position r; this is our simple model of the negative charge on an adsorbed surface species. This is balanced by a charge of $-\sigma_2$, also at $z = L$. If we sum these fields shown in Figure 5b, we see there are now two distinct regions of field. Integrating the field gives the green curve shown in Figure 5c, where we can immediately see that the presence of the charged adsorbate perturbs the surface potential (at $z = 0$).

To relate this to our first interpretation, we will start with a question: By how much do we need to adjust σ_1 in order to keep the electrode potential constant when the charge σ_2 is introduced? We can quickly deduce that in this simple model, where the required charge is $n = -\frac{L-r}{L}$, as shown in Supporting Information section S3.3. The second interpretation asks, How much of an applied change in potential does our charge (σ_2) "feel"? This is equivalent to the partial derivative,

$$\delta = \left(\frac{\partial \phi(r)}{\partial \phi(0)} \right)_{r,L,\sigma_2} \qquad (7)$$

We can quickly work out this derivative for our model, finding $d = \frac{L-r}{L}$, also shown in Supporting Information section S3.3. Thus, we can now identify that $\delta = -n$, and the two interpretations (expressed earlier in eqs 3 and 5) are equivalent. Therefore, studying the potential-dependence of the pK_a allows us to deduce the amount of electron transfer that is coupled with the protonation, as well as to understand the potential drop at the point of the charge.

Interestingly, this model implies that if the charged species were moved closer to the electrode, then we should expect the non-integer charge transfer (n) to be larger. The mercaptobenzoic acid molecule lends itself to such inquiry: for example, if the functional group is moved from the *para-* to the *ortho-* position we expect n to increase. An experimental measurement of 2-MBA exists in the literature[22] (albeit on a Ag, not Au, surface) which provides a natural test of this model prediction. To complete this comparison, we also performed grand-canonical electronic-structure calculations on 2-MBA, and we found n to increase in magnitude to about −0.6, from about −0.1 for 4-MBA. We found the prediction of the pK_a−potential slope to again be in close agreement with that measured. Details are included in Supporting Information section S2.8, and a slope comparison is given in Figure S10.

CONCLUSION

In summary, this study gives us a simple and unified means to interpret the thermodynamics of proton transfer at the electrified surface. By studying a system where the potential-dependence of the pK_a can be spectroscopically observed, we can deduce the thermodynamics of the coupled proton–electron transfer process for the general case where the electron is not necessarily an integer. The agreement between the experimental measurements and electronic-structure calculations should give confidence in the use of electronic-structure calculations in reactions where the intermediates are not readily measurable, such as in the kinetically relevant steps H$_2$ evolution or CO$_2$ reduction. Further, the unified agreement between the two interpretations gives us an intuitive means to understand charge transfer at the electrified interface.

ASSOCIATED CONTENT

Supporting Information

The Supporting Information is available free of charge at https://pubs.acs.org/doi/10.1021/jacs.0c03472.

> Extended methods description, extended results analysis, and Gauss's law model (PDF)

AUTHOR INFORMATION

Corresponding Authors

Tianquan Lian − *Department of Chemistry, Emory University, Atlanta, Georgia 30322, United States;* orcid.org/0000-0002-8351-3690; Email: tlian@emory.edu

Andrew A. Peterson − *School of Engineering, Brown University, Providence, Rhode Island 02912, United States;* orcid.org/0000-0003-2855-9482; Email: andrew_peterson@brown.edu

Authors

Aimin Ge − *Department of Chemistry, Emory University, Atlanta, Georgia 30322, United States;* orcid.org/0000-0003-0127-3193

Georg Kastlunger − *School of Engineering, Brown University, Providence, Rhode Island 02912, United States*

Jinhui Meng − *Department of Chemistry, Emory University, Atlanta, Georgia 30322, United States*

Per Lindgren − *School of Engineering, Brown University, Providence, Rhode Island 02912, United States*

Jia Song − *Department of Chemistry, Emory University, Atlanta, Georgia 30322, United States*

Qiliang Liu − *Department of Chemistry, Emory University, Atlanta, Georgia 30322, United States*

Alexander Zaslavsky − *School of Engineering, Brown University, Providence, Rhode Island 02912, United States*

Complete contact information is available at:
https://pubs.acs.org/10.1021/jacs.0c03472

Author Contributions

[⊥]Aimin Ge and Georg Kastlunger contributed equally.

Notes

The authors declare no competing financial interest.

REFERENCES

(1) Schultze, J. W.; Vetter, K. J. Experimental determination and interpretation of the electrosorption valency γ. *J. Electroanal. Chem. Interfacial Electrochem.* **1973**, *44*, 63−81.

(2) Schmickler, W.; Guidelli, R. The partial charge transfer. *Electrochim. Acta* **2014**, *127*, 489−505.

(3) Horányi, G.; Láng, G. Double-layer phenomena in electrochemistry: Controversial views on some fundamental notions related to electrified interfaces. *J. Colloid Interface Sci.* **2006**, *296*, 1−8.

(4) Joo, J.; Uchida, T.; Cuesta, A.; Koper, M. T. M.; Osawa, M. Importance of Acid-Base Equilibrium in Electrocatalytic Oxidation of Formic Acid on Platinum. *J. Am. Chem. Soc.* **2013**, *135*, 9991−9994.

(5) Yaguchi, M.; Uchida, T.; Motobayashi, K.; Osawa, M. Speciation of Adsorbed Phosphate at Gold Electrodes: A Combined Surface-Enhanced Infrared Absorption Spectroscopy and DFT Study. *J. Phys. Chem. Lett.* **2016**, *7*, 3097−3102.

(6) Gan, S.; Zhong, L.; Gao, L.; Han, D.; Niu, L. Electrochemically Driven Surface-Confined Acid/Base Reaction for an Ultrafast H⁺ Supercapacitor. *J. Am. Chem. Soc.* **2016**, *138*, 1490−1493.

(7) Bishnoi, S. W.; Rozell, C. J.; Levin, C. S.; Gheith, M. K.; Johnson, B. R.; Johnson, D. H.; Halas, N. J. All-optical nanoscale pH meter. *Nano Lett.* **2006**, *6*, 1687−1692.

(8) Talley, C. E.; Jusinski, L.; Hollars, C. W.; Lane, S. M.; Huser, T. Intracellular pH Sensors Based on Surface−Enhanced Raman Scattering. *Anal. Chem.* **2004**, *76*, 7064−7068.

(9) Wang, W.; Zhao, F.; Li, M.; Zhang, C.; Shao, Y.; Tian, Y. A SERS Optophysiological Probe for the Real−Time Mapping and Simultaneous Determination of the Carbonate Concentration and pH Value in a Live Mouse Brain. *Angew. Chem., Int. Ed.* **2019**, *58*, 5256−5260.

(10) Eisenthal, K. B. Liquid Interfaces Probed by Second-Harmonic and Sum-Frequency Spectroscopy. *Chem. Rev.* **1996**, *96*, 1343−1360.

(11) Cheng, S. S.; Scherson, D. A.; Sukenik, C. N. In Situ Attenuated Total Reflectance Fourier Transform Infrared Spectroscopy of Carboxylate-Bearing, Siloxane-Anchored, Self-Assembled Monolayers: A Study of Carboxylate Reactivity and Acid-Base Properties. *Langmuir* **1995**, *11*, 1190−1195.

(12) Koivisto, J.; Chen, X.; Donnini, S.; Lahtinen, T.; Häkkinen, H.; Groenhof, G.; Pettersson, M. Acid-base properties and surface charge distribution of the water-soluble Au$_{102}$(pMBA)$_{44}$ nanocluster. *J. Phys. Chem. C* **2016**, *120*, 10041−10050.

(13) Wang, D.; Nap, R. J.; Lagzi, I.; Kowalczyk, B.; Han, S.; Grzybowski, B. A.; Szleifer, I. How and Why Nanoparticle's Curvature Regulates the Apparent pKa of the Coating Ligands. *J. Am. Chem. Soc.* **2011**, *133*, 2192−2197.

(14) Smith, C. P.; White, H. S. Voltammetry of Molecular Films Containing Acid/Base Groups. *Langmuir* **1993**, *9*, 1−3.

(15) White, H. S.; Peterson, J. D.; Cui, Q.; Stevenson, K. J. Voltammetric Measurement of Interfacial Acid/Base Reactions. *J. Phys. Chem. B* **1998**, *102*, 2930−2934.

(16) Burgess, I.; Seivewright, B.; Lennox, R. B. Electric field driven protonation/deprotonation of self-assembled monolayers of acid-terminated thiols. *Langmuir* **2006**, *22*, 4420−4428.

(17) Rosendahl, S. M.; Burgess, I. J. Electrochemical and infrared spectroscopy studies of 4-mercaptobenzoic acid SAMs on gold surfaces. *Electrochim. Acta* **2008**, *53*, 6759−6767.

(18) Luque, A. M.; Mulder, W. H.; Calvente, J. J.; Cuesta, A.; Andreu, R. Proton Transfer Voltammetry at Electrodes Modified with Acid Thiol Monolayers. *Anal. Chem.* **2012**, *84*, 5778−5786.

(19) Lounasvuori, M. M.; Holt, K. B. Acid deprotonation driven by cation migration at biased graphene nanoflake electrodes. *Chem. Commun.* **2017**, *53*, 2351−2354.

(20) Luque, A. M.; Cuesta, A.; Calvente, J. J.; Andreu, R. Potentiostatic infrared titration of 11-mercaptoundecanoic acid monolayers. *Electrochem. Commun.* **2014**, *45*, 13−16.

(21) Sugihara, K.; Shimazu, K.; Uosaki, K. Electrode potential effect on the surface pKa of a self-assembled 15-mercaptohexadecanoic acid monolayer on a gold/quartz crystal microbalance electrode. *Langmuir* **2000**, *16*, 7101−7105.

(22) Ma, C.; Harris, J. M. Surface-enhanced raman spectroscopy investigation of the potential-dependent acid-base chemistry of silver-immobilized 2-mercaptobenzoic acid. *Langmuir* **2011**, *27*, 3527−3533.

(23) Cao, X. W. Study of electrode potential effect on acid-base behavior of ω-functionalized self-assembled monolayers using Fourier transform surface-enhanced Raman scattering spectroscopy. *J. Raman Spectrosc.* **2005**, *36*, 250−256.

(24) Gouy, M. Sur la constitution de la charge électrique à la surface d'un électrolyte. *J. Phys. Theor. Appl.* **1910**, *9*, 457−468.

(25) Chapman, D. L. LI. A contribution to the theory of electrocapillarity. *London, Edinburgh, and Dublin Philosophical Magazine and Journal of Science* **1913**, *25*, 475−481.

(26) Frumkin, A.; Petry, O.; Damaskin, B. The notion of the electrode charge and the Lippmann equation. *J. Electroanal. Chem. Interfacial Electrochem.* **1970**, *27*, 81−100.

(27) Schmickler, W.; Henderson, D. The interphase between jellium and a hard sphere electrolyte: Capacity-charge characteristics and dipole potentials. *J. Chem. Phys.* **1986**, *85*, 1650−1657.

(28) Schmickler, W.; Guidelli, R. Ionic adsorption and the surface dipole potential. *J. Electroanal. Chem. Interfacial Electrochem.* **1987**, *235*, 387−392.

(29) Schmickler, W. The surface dipole moment of species adsorbed from a solution. *J. Electroanal. Chem. Interfacial Electrochem.* **1988**, *249*, 25−33.

(30) Kornyshev, A. A.; Schmickler, W. On the coverage dependence of the partial charge transfer coefficient. *J. Electroanal. Chem. Interfacial Electrochem.* **1986**, *202*, 1−21.

(31) Bange, K.; Straehler, B.; Sass, J. K.; Parsons, R. The interaction of Br with Ag (110): comparison of electrochemical and gas-phase adsorption measurements. *J. Electroanal. Chem. Interfacial Electrochem.* **1987**, *229*, 87−98.

(32) Kornyshev, A. A.; Vorotyntsev, M. A. Field-induced interfacial relaxation and electrical properties of the compact layer. *J. Electroanal. Chem. Interfacial Electrochem.* **1984**, *167*, 1−14.

(33) Wang, F.; Widejko, R. G.; Yang, Z.; Nguyen, K. T.; Chen, H.; Fernando, L. P.; Christensen, K. A.; Anker, J. N. Surface-Enhanced Raman Scattering Detection of pH with Silica-Encapsulated 4-Mercaptobenzoic Acid-Functionalized Silver Nanoparticles. *Anal. Chem.* **2012**, *84*, 8013−8019.

(34) Pienpinijtham, P.; Vantasin, S.; Kitahama, Y.; Ekgasit, S.; Ozaki, Y. Nanoscale pH profile at a solution/solid interface by chemically modified tip-enhanced raman scattering. *J. Phys. Chem. C* **2016**, *120*, 14663−14668.

(35) Wells, M.; Dermody, D. L.; Yang, H. C.; Kim, T.; Crooks, R. M.; Ricco, A. J. Interactions between Organized, Surface-Confined Monolayers and Vapor-Phase Probe Molecules. 9. Structure/Reactivity Relationship between Three Surface-Confined Isomers of Mercaptobenzoic Acid and Vapor-Phase Decylamine. *Langmuir* **1996**, *12*, 1989−1996.

(36) Michota, A.; Bukowska, J. Surface-enhanced Raman scattering (SERS) of 4-mercaptobenzoic acid on silver and gold substrates. *J. Raman Spectrosc.* **2003**, *34*, 21−25.

(37) Borkovec, M.; Koper, G. J. M. Ising models and acid-base properties of weak polyelectrolytes. *Ber. Bunsen-Ges. Phys. Chem.* **1996**, *100*, 764−769.

(38) Borkovec, M. Origin of 1−pK and 2−pK Models for Ionizable Water−Solid Interfaces. *Langmuir* **1997**, *13*, 2608−2613.

(39) Kakiuchi, T.; Iida, M.; Imabayashi, S.-i.; Niki, K. Double−Layer−Capacitance Titration of Self−Assembled Monolayers of ω−Functionalized Alkanethiols on Au(111) Surface. *Langmuir* **2000**, *16*, 5397−5401.

(40) Trasatti, S.; Parsons, R. Interphases in systems of conducting phases (Recommendations 1985). *Pure Appl. Chem.* **1986**, *58*, 437.

(41) Kastlunger, G.; Lindgren, P.; Peterson, A. A. The controlled-potential simulation of elementary electrochemical reactions: proton discharge on metal surfaces. *J. Phys. Chem. C* **2018**, *122*, 12771−12781.

(42) Mulliken, R. S. Electronic population analysis on LCAO-MO molecular wave functions. I. *J. Chem. Phys.* **1955**, *23*, 1833−1840.

(43) Bader, R. F. W. Atoms in molecules. *Acc. Chem. Res.* **1985**, *18*, 9−15.

(44) Reed, A. E.; Weinstock, R. B.; Weinhold, F. Natural population analysis. *J. Chem. Phys.* **1985**, *83*, 735−746.

(45) Smith, C. P.; White, H. S. Theory of the interfacial potential distribution and reversible voltammetric response of electrodes coated with electroactive molecular films. *Anal. Chem.* **1992**, *64*, 2398−2405.

(46) Stern, O. Zur Theorie der Elektrolytischen Doppelschicht. *Zeitschrift fur Elektrochemie* **1924**, *30*, 508−516.

(47) Carnie, S. L.; Chan, D. Y. The modelling of solvent structure in the electrical double layer. *Adv. Colloid Interface Sci.* **1982**, *16*, 81−100.

(48) Rossmeisl, J.; Skúlason, E.; Björketun, M. E.; Tripkovic, V.; Nørskov, J. K. Modeling the electrified solid-liquid interface. *Chem. Phys. Lett.* **2008**, *466*, 68−71.

(49) Chan, K.; Nørskov, J. K. Electrochemical Barriers Made Simple. *J. Phys. Chem. Lett.* **2015**, *6*, 2663−2668.

(50) Gauthier, J. A.; Dickens, C. F.; Heenen, H. H.; Vijay, S.; Ringe, S.; Chan, K. Unified Approach to Implicit and Explicit Solvent Simulations of Electrochemical Reaction Energetics. *J. Chem. Theory Comput.* **2019**, *15*, 6895−6906.